

Absorbing Markov Chain Saliency Driven Active Contour Model for Digital Image Boundary Extraction

Muhammad Syukri Mazlin¹, Abdul Kadir Jumaat² and Rohana Embong³

^{1, 2, 3} School of Mathematical Sciences, College of Computing, Informatics and Mathematics, Universiti Teknologi MARA, Shah Alam, Malaysia

² Institute for Big Data Analytics and Artificial Intelligence (IBDAAI), Universiti Teknologi MARA, 40450, Shah Alam, Selangor, Malaysia

*corresponding author: ²abdulkadir@tmsk.uitm.edu.my

ARTICLE HISTORY

ABSTRACT

Received
19 June 2023

Accepted
20 August 2023

Available online
30 September 2023

The image segmentation approach using the active contour model (ACM) has achieved notable success in digital image analysis for extracting image boundaries. The region-based ACM can be divided into two classes: global segmentation and selective segmentation. Global segmentation, in which all desired boundaries of targeted objects are extracted from an input image, is preferable to the selective model due to its high utility, particularly in shape analysis. However, when segmenting a digital image with inhomogeneous intensity, the global ACM appears to produce unsatisfactory results. Thus, this research provides a new global ACM for segmenting digital images with an inhomogeneous intensity incorporating an absorption Markov chain (AMC) saliency image map and local image fitting principles. In addition, the Euler-Lagrange (EL) Partial Differential equation for solving the proposed model was provided. Thirty sets of digital images were used to validate the model. The accuracy of the proposed model, as indicated by Dice and Jaccard values, is approximately 3.81% and 10.63% higher, respectively, than that of the competing model, as determined by numerical analysis. In addition, the segmentation process taken by the proposed model is faster than the existing model. The proposed model has high potential to be extended into colour and multiphase formulations in future research.

Keywords: active contour; boundary extraction; global segmentation; saliency map; intensity inhomogeneity.

1. INTRODUCTION

In numerous image processing and computer vision applications, including medical imaging [1–4] and object recognition [5–7], the extraction of image boundaries for subsequent processing and analysis is a crucial step. This method is also referred to as image segmentation. There are two distinct categories of segmentation methods: variational and non-variational. Despite being effective for simple images, non-variational approaches such as thresholding and region-growing methods, are ineffective for handling topological changes, whereas the non-variational machine learning-based method [8] requires a significant quantity of data that is typically unavailable. Variational approaches have been demonstrated to be effective in image segmentation and are less dependent on the quantity of data.

Active contour models (ACM) are the most popular method in the variational approach due to applying the calculus of variations and optimisation procedures to minimise the energy cost

function. Variational ACM can be divided into two types: edge-based and region-based strategies. Kass et al. [9] proposed the most renowned edge-based variational ACM by applying the explicit snake model to a conventional parametric curve. This technique is, however, sensitive to image disturbance. In contrast, the region-based variational ACM utilises image information such as shape, texture characteristics, and pixel intensities in a global or local area to converge contour curves into acceptable target borders [10–12]. The region-based variational ACM method is less susceptible to image disturbance and is more adept at handling topological changes than the edge-based method. Region-based variational ACM can be divided into global and selective segmentation classes.

Selective segmentation is extracting a single object from a set of digital images. Selective segmentation models such as [13–14] have produced unsatisfactory results for digital images containing multiple targeted objects. To resolve this issue, it is preferable to employ global segmentation techniques that seek to segment all objects within the input image. Mumford and Shah's [15] model is a well-known variational global ACM. Due to the difficulty in solving the model, Chan and Vese [16] reformulated the Mumford-Shah model as the Chan-Vese (CV) model, a straightforward, numerical representation without approximation. This CV model has two phases representing the image's background and foreground; it is a special case of the piecewise constant (PC) model. However, the CV model is ineffective for segmenting images with inhomogeneous intensity because its mathematical formulation is based on global image intensity information.

In the realm of image segmentation, intensity inhomogeneity is a major constraint. This refers to variations in image intensity values within a single digital image, making distinguishing between the foreground and background of the targeted objects difficult for experts, resulting in incorrect decisions.

To solve the problem of segmenting an image with inhomogeneous intensity, the Local Binary Fitting (LBF) model [17] was developed, which uses the local image intensity. While the LBF model produces effective segmentation results, its formulation's computational complexity increases the computation time. The Local Image Fitting (LIF) model [18] was introduced to circumvent limitations of the LBF model. Since then, numerous researchers have used the concept of local image intensity in image segmentation to handle images with inhomogeneous intensity, such as [19–21].

In addition to using local image intensity to obtain improved results for images with intensity inhomogeneity, researchers are currently noticing the saliency map concept. Saliency generally refers to the quality of being noticeable by emphasising the area to which people will direct their attention first. According to [22], the saliency map is derived from visual distinction and astonishment. In other words, this saliency map will aid in determining the initial contour of the object of interest, as its initial estimate can readily separate the object from the background. Several investigations have incorporated the saliency map concept into their models. For instance, Zhi and Shen [22] conducted a study titled “Saliency-Driven Region-Edge-Based Top-Down Level Set Evolution (SDREL)”, where they demonstrated that the concept of using the saliency map can lead to a more accurate and effective segmentation result. However, Iqbal et al. [21] asserted that the previously mentioned model is ineffective at segmenting an image with severe intensity heterogeneity. They developed a new segmentation model dubbed the Local Saliency Fitting (LSF) by incorporating the saliency image map with the local image

intensity concept. Unfortunately, the traditional saliency function used to compute the saliency image map may have overlooked some crucial structures in low-contrast digital images. The formulation produces artefacts or image noise for digital images with high contrast. These deficiencies result in unsatisfactory digital image boundary extraction output.

As a result, this research will present a global kind of ACM to effectively extract the digital image's boundaries by modifying the LFS model using the saliency image map function in the LSF model produced via the absorbing Markov chain (AMC) approach [23]. By modifying the LSF model, an enhancement in segmentation accuracy and efficiency is anticipated.

The subsequent section of this study provides a concise summary of the LSF model, which is closely related to this investigation. The suggested model's formulation and solution are then explored. The experimental results of both the LFS and the suggested models are provided.

2. THE LSF MODEL

The LSF model [21] is a global type of ACM which aims to extract all targeted object boundaries in a digital image. Let I be the input image. In the model, the saliency image map S is computed using the following Equation 1:

$$S(\Omega) = |I_{avg} - I_{filter}(\Omega)|, \quad \Omega = (x, y) \quad (1)$$

Where the average of I in domain Ω is denoted by I_{avg} while output of I after implementing Gaussian filter for noise removal is denoted by $I_{filter}(x, y)$. Then, the saliency-driven local fitted image S_{LSF} is defined using the following Equation 2:

$$S_{LSF}(x) = L_{s1}(x)H_1 + L_{s2}(x)H_2 \quad (2)$$

The terms $H_1 = H(\phi)$ and $H_2 = 1 - H(\phi)$ are the Heaviside functions and the term L_{s1} and L_{s2} are the average of intensity based on S the inside and outside of the generated contour ϕ that defines the extracted boundaries of a digital image, respectively. By incorporating the total variation function and distance regularising function, the final formulation of the LSF derived using the calculus of variation approach is defined as Equation 3 as follows:

$$\begin{aligned} \frac{\partial \phi}{\partial t} = & \left[(S - S_{LSF})(L_{s1} - L_{s2})\delta(\phi) \right] + \mu \left(\Delta \phi - \text{div} \left(\frac{\nabla \phi}{|\nabla \phi|} \right) \right) \\ & + \left[(I - I_{LIF})(m_1 - m_2)\delta(\phi) \right] + \nu \cdot \text{div} \left(\frac{\nabla \phi}{|\nabla \phi|} \right) \end{aligned} \quad (3)$$

The first term represents the saliency driven energy while the local image function is denoted by the third term. These terms can drive the generated contour towards the boundaries of the targeted objects. The second term is the distance regularising function, and the last term is the contour length, where these terms ensure the smoothness of the extracted image boundaries. Although the model ", and the saliency term in Equation 1 potentially missed some important

features of a digital image, especially when dealing with low-contrast images. In addition, it often highlights some unneeded small regions called image noise in the targeted objects or the backgrounds. Consequently, these yield an unsatisfactory segmentation result.

3. METHODOLOGY

In this section, the description of the research methodology is explained based on the flow chart in Figure 1 as follows.

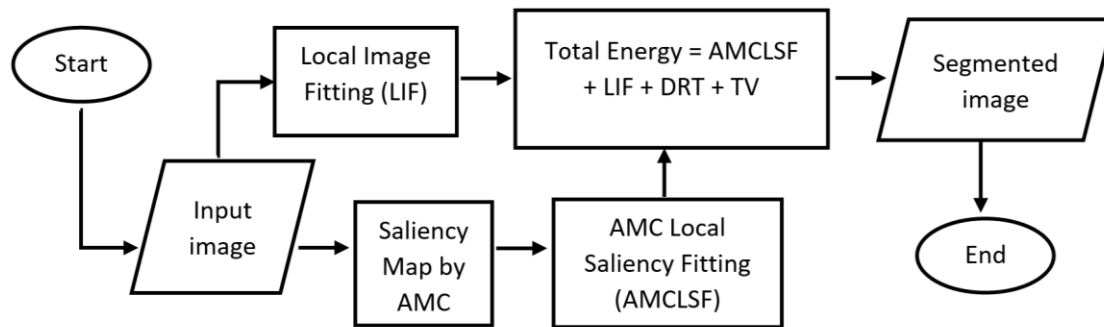


Figure 1: Flowchart of the proposed model

Initially, the AMC-based saliency map and LIF energy of an input image were computed based on Figure 1. Next, the computed saliency map was used to derive the AMC-based LSF energy (AMCLSF). This important part distinguishes existing works such as [21] and [22] that use the traditional saliency function to compute the saliency map, while this new proposed model utilises the AMC method to compute the saliency map. The significance of utilising the AMC method is demonstrated in Section 3.2. A total energy minimisation function representing the new model was then developed to segment the input image by integrating the AMCLSF and LIF energies with the distance regularisation term (DRT) and length term, also known as the total variation (TV) function, which aims to identify and segment the objects or regions within an input image and produce a better saliency map image that is particularly useful for any global segmentation method. In the following section, each stage is described in detail.

3.1 Input Image

This study collected 30 sets of test images from [24] and [25]. The image dimension of 128 by 128 pixels was utilised for all test images. In addition, the test images had varying intensities to ensure that the proposed model met its objective. All the benchmarks for the test images were derived from the same sources.

3.2 Saliency Map via Absorbing Markov Chain

The saliency detection method using the absorbing Markov chain computes the probability of a random walker being absorbed by various states in an image using a Markov chain model. There are two distinct states at play: the absorbing states r and the transient states t . The concept is that a state with a high probability of absorption represents a salient region in the image because it attracts the random walker more than other states. These probabilities can be represented as a matrix, with matrix Q representing the transition probabilities between transient states, matrix R representing the transition probabilities from transient to absorbing

states, and matrix I representing the transition probabilities between absorbing rates. Consequently, the transition matrix P can be defined as $P \rightarrow \begin{pmatrix} Q & R \\ 0 & I \end{pmatrix}$. Beginning with constructing an image graph, each node represents a superpixel, and each edge connects two adjacent superpixels. The formula for calculating the absorbed time for each transient state is $y = N \times c$. Here, matrix c is the t dimensional column vector whose elements are 1, and matrix N is the fundamental matrix of the absorbing Markov chain, given by $N = (I - Q)^{-1}$. From this graph, the transition matrix of the Markov chain was computed, and the absorbing probability of each state was determined using the theory of absorbing Markov chains. The resultant probabilities were then used as the image's saliency map. The absorbing state corresponded to the final saliency map, and the transition probabilities between states were learned from the input image data, enabling the algorithm to determine which regions were more conspicuous (salient). According to [23], the saliency map based on the AMC technique, S_{AMC} can be acquired by normalising the absorbed time equation $y = N \times c$ and is given by Equation 4.

$$S_{AMC}(i) = y(i) \quad i = 1, 2, \dots, t \quad (4)$$

Here, i it indicates the graph indexing for transient nodes. This method has been demonstrated to be effective at identifying salient regions. As shown in Figure 2, the saliency results derived from the LSF model [21] and the AMC were compared to bolster our claim.

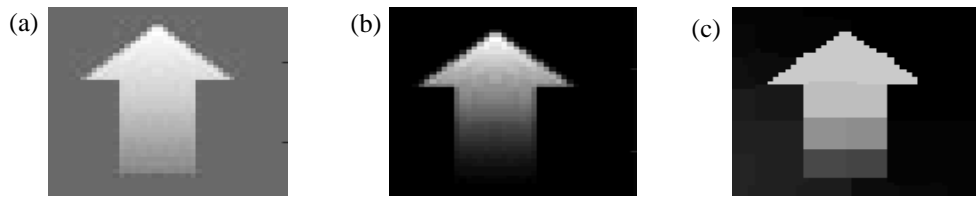


Figure 2: The comparison of the saliency map images by the LIF model and AMC technique (a) Input image (b) Saliency map by LIF model (c) Saliency map using AMC

According to Figure 2, the input image is a synthetic intensity inhomogeneity image. From visual inspection, it is evident that the saliency detection method generated by the AMC technique [23] is more optimal and efficient for use in this study, as it can generate a more salient image result than [21].

3.3 Local Image Fitting

This study's local image fitting is computed using the Local Image Fitting (LIF) model [18]. The local image fitting is important to handle images with intensity inhomogeneity. Assuming that for an image $I = I(x, y)$ in a domain Ω , the regularised local image fitting energy function in the level set formulation E_ϵ^{LIF} is defined in Equation 5 as follows:

$$E_\epsilon^{LIF}(\phi) = \frac{1}{2} \int_{\Omega} |I - I^{LIF}|^2 dx dy \quad (5)$$

The fitted image $I^{LIF} = I^{LIF}(x, y)$ in Equation 5 can be written as $I^{LIF} = n_1H_1 + n_2H_2$. Here, n_1 and n_2 are the intensity averages of the interior and exterior in a local region by defining a truncated Gaussian window $W_k(x, y)$ with a standard deviation σ and a radius κ of kernel window. In practical applications, the value of standard deviation is essential where it should be correctly selected based on the images. If the setting parameter σ is set to be small, it may provide incorrect results, whereas a value σ that is too large will result in a high computational cost.

3.4 AMC-based Local Saliency Fitting

The LIF term is not enough to handle images with severe intensity inhomogeneity. In this research, another term is proposed to handle the problem termed AMC-based Local Saliency Fitting (AMCLSF), which is based on Equation 4 and Equation 5, defined as the following Equation 6:

$$AMCLSF(\phi) = \frac{1}{2} \int_{\Omega} |S_{AMC} - S_{AMC}^{LIF}|^2 dx dy \quad (6)$$

Here, we defined $S_{AMC}^{LIF} = m_1H_1 + m_2H_2$ such that.

$$\begin{cases} m_1 = \text{mean}\left(S_{AMC} \in \left(\{(x, y) \in \Omega \mid \phi(x, y) > 0\} \cap W_k(x, y)\right)\right) \\ m_2 = \text{mean}\left(S_{AMC} \in \left(\{(x, y) \in \Omega \mid \phi(x, y) < 0\} \cap W_k(x, y)\right)\right) \end{cases}$$

Where m_1 and m_2 represent the AMC saliency-based intensity average for the inside and outside of the segmentation contour ϕ in a local region by defining a truncated Gaussian window $W_k(x, y)$ with a standard deviation σ and a radius κ of kernel window. The AMCLSF enables the extraction of accurate local image information, especially for images with inhomogeneous intensity, to increase segmentation accuracy.

3.5 Total Energy Functional

This step proposes a novel energy functional, a new variational global ACM called the absorbing Markov chain saliency-based active contour (AMCSAC) model. The proposed AMCSAC model consists of the combination of Equations 5 and 6. In addition, the total variation function $TV = \int_{\Omega} \delta(\phi) |\nabla \phi| dx dy$ is introduced to generate a smooth curve. A distance regularisation term $DRT = \int_{\Omega} \frac{1}{2} (|\nabla \phi| - 1)^2 dx dy$ is also added in the AMCSAC model to stabilise the evolution of the generated segmentation contour. With all these ingredients, the AMCSAC model in the level-set formulation is defined in Equation 7 as follows:

$$\begin{aligned} \min_{\phi} AMCSAC(\phi) &= \frac{1}{2} \int_{\Omega} [I - (n_1 H_1 + n_2 H_2)^2] d\Omega + \mu \int_{\Omega} \frac{1}{2} (|\nabla \phi| - 1)^2 d\Omega \\ &+ \frac{1}{2} \int_{\Omega} [S_{AMC} - (m_1 H_1 + m_2 H_2)^2] d\Omega + \nu \int_{\Omega} \delta(\phi) |\nabla \phi| d\Omega \end{aligned} \quad (7)$$

Here, the integers $\mu > 0$ and $\nu > 0$ are the parameters to weigh the DF, DRT and TV functions, respectively. To solve the model, the Euler-Lagrange partial differential equation is derived, which is defined as the following Equation 8:

$$\begin{aligned} \frac{\partial \phi}{\partial t} &= \left[(S_{AMC} - S_{AMC}^{LIF})(m_1 - m_2) \delta(\phi) \right] + \mu \left(\Delta \phi - \operatorname{div} \left(\frac{\nabla \phi}{|\nabla \phi|} \right) \right) \\ &+ \left[(I(x) - I^{LIF}(x))(n_1 - n_2) \delta(\phi) \right] + \nu \cdot \delta \operatorname{div} \left(\frac{\nabla \phi}{|\nabla \phi|} \right) \end{aligned} \quad (8)$$

3.6 Algorithm's Step for the AMCSAC model

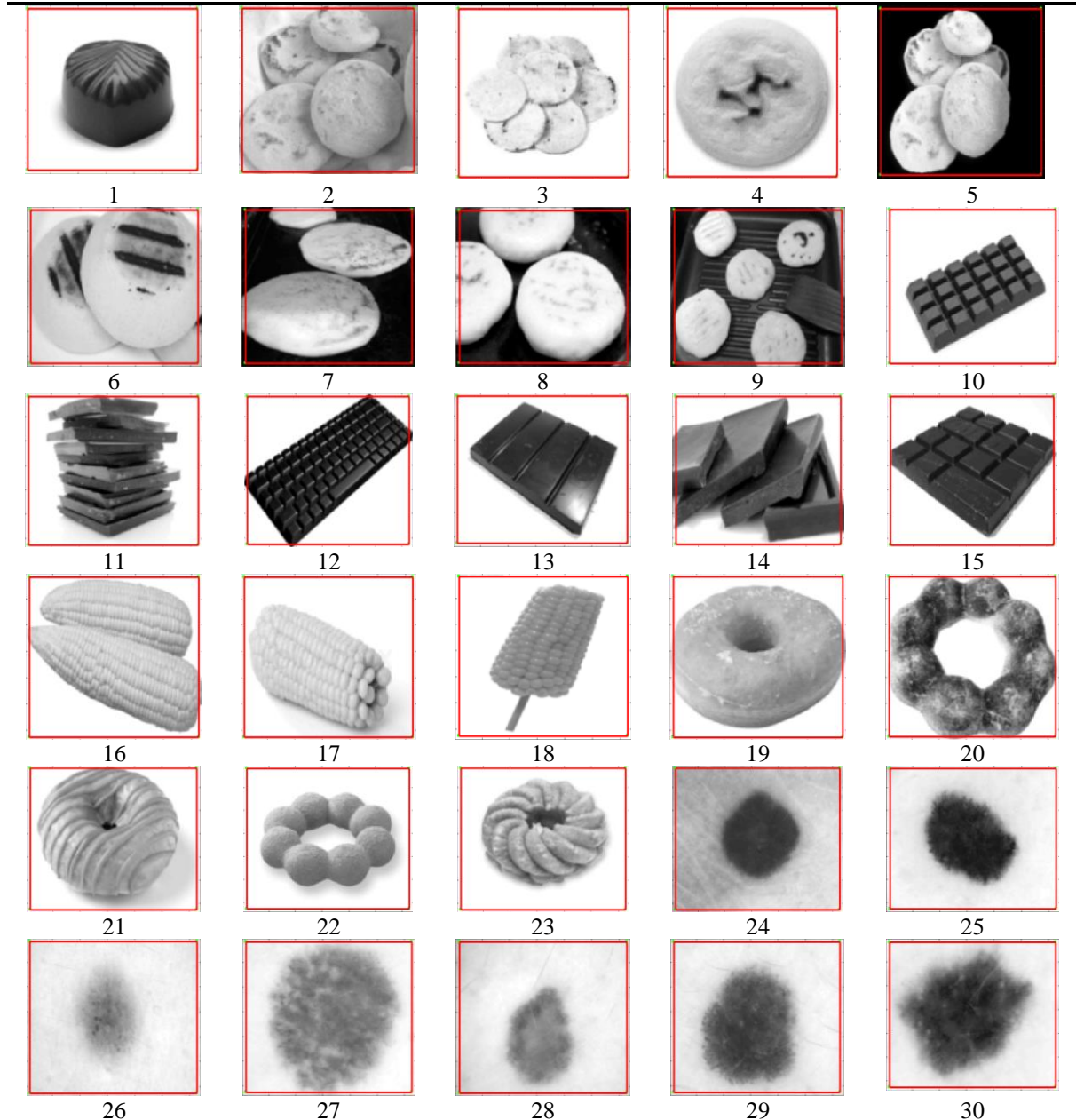
To compute the solution of Equation 8 that represents the Euler-Lagrange partial differential equation of the proposed AMCSAC model, MATLAB R2021a software was used. To stop the program automatically, the constant $maxit=200$ was used as the iterations number and a tolerance value $tol = 1 \times 10^{-5}$ is defined. It is remarked that the saliency image map via the AMC method is used in this research to replace the traditional saliency function where the final formulation of the saliency map energy functional is computed as in Equation 4. Thus, the following algorithm outlines the process for implementing the new proposed AMCSAC model:

- Step 1: Input the test image.
- Step 2: Set values of tol , $max it$, and σ .
- Step 3: The initial segmentation curve is defined around the targeted object.
- Step 4: Evaluate the saliency map, S_{AMC} , from Equation 4.
- Step 5: **For** iteration=1 to $max it$ or $\|\phi^{n+1} - \phi^n\|/\|\phi^n\| \leq tol$ **do**
Generate the function ϕ , which is the zero-level set function based on Equation 8.
- Step 6: The final segmentation curve of the extracted object's boundaries will be the output ϕ .

4. RESULTS AND DISCUSSION

Table 1 below shows all 30 test images with the initial contour in red used in this experiment.

Table 1: Test images with initial contours



From Table 1, images 1 until 23 are food images, while images 24 until 30 are medical images. These images were chosen because all the test images have their intensity inhomogeneity features. Thus, they are very difficult to segment. Hence, all the images chosen were significant in testing the performance of the proposed model. The segmentation process was run using MATLAB software, and the segmentation results of all 30 test images between the proposed AMCSAC model and the LSF model done by [18] were compared. The visual illustration of

the segmentation result and the saliency image for the chosen six test images (out of 30 images) are demonstrated in the following Table 2.

Table 2: Segmentation Result


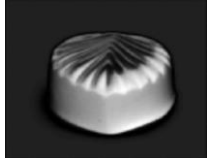





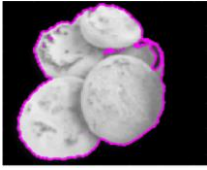

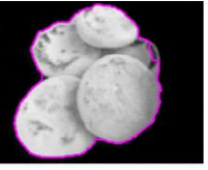



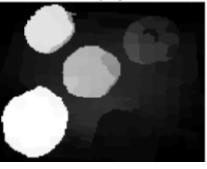


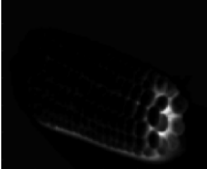


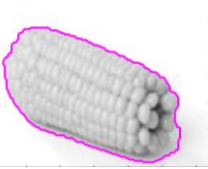



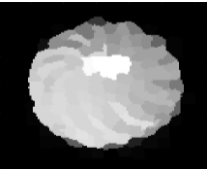

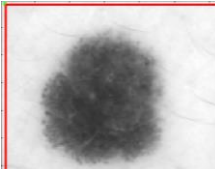
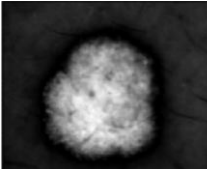
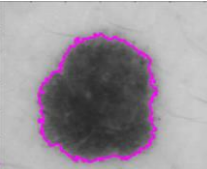

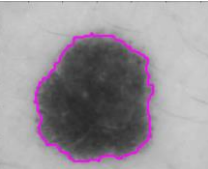
Input images with initial contour	LSF Model		AMCSAC model	
	Saliency Output	Segmentation Output	Saliency Output	Segmentation Output
				
1	1a	1b	1c	1d
				
5	5a	5b	5c	5d
				
9	9a	9b	9c	9d
				
17	17a	17b	17c	17d
				
23	23a	23b	23c	23d
				
29	29a	29b	29c	29d

Table 2 presents the saliency output of the LSF and AMCSAC models in the second and fourth columns, respectively. The segmentation results of the LSF and the AMCSAC models,

illustrated by the purple curve line, are located in the third and last columns, respectively. The results represent the extracted boundaries of the targeted objects in the given images.

By visual observation, both models could segment all the test images. However, both produced different segmentation results. It can be observed that the segmentation results for the LSF model in Table 2 (1b, 9b, 17b, and 23b) produced unnecessary noises, which made the final contour more scattered. In addition, the saliency image produced by the LSF model is a bit darker, which made it more difficult for the model to make a near-optimal initial guess.

Unlike the segmentation result produced by the proposed model, where the final contour is smoother, and the saliency image produced is better, the image's object and foreground can be distinguished thanks to the absorbing Markov chain approach. This is particularly for modelling and analysing systems with absorbing states that offer a robust framework where the absorbing state represent the most salient areas on the saliency maps. This technique guarantees the reliability and consistency of the produced saliency map [23].

Besides the qualitative visual observation, this experiment will be judged based on the quantitative accuracy measures using the Dice Similarity Coefficient (DSC) and Jaccard Similarity Coefficient (JSC). The return value of DSC and JSC close to 1 indicates good boundary extraction quality. The value close to 0 indicates poor boundary extraction quality. The processing time was also recorded to determine the efficiency of the LSF and AMCSAC models. Table 3 displays both models' processing time, DSC, and JSC in segmenting all 30 digital images.

Table 3: Processing Time, JSC and DSC

Input Images	LSF Model			AMCSAC model		
	Time	DSC	JSC	Time	DSC	JSC
1	30.2872	0.9552	0.9142	29.9243	0.9640	0.9304
2	32.0377	0.4633	0.3015	30.1129	0.4815	0.3171
3	30.7858	0.5221	0.3532	31.5829	0.5898	0.4183
4	29.8684	0.8409	0.7255	29.9456	0.8766	0.7802
5	31.6948	0.9638	0.9302	29.9383	0.9700	0.9417
6	29.8459	0.3582	0.2182	29.8006	0.3776	0.2327
7	30.7122	0.9637	0.9299	30.3419	0.9714	0.9443
8	33.7468	0.9469	0.8992	29.9353	0.9558	0.9154
9	41.3756	0.8990	0.8165	48.9182	0.9087	0.8327
10	33.6000	0.9625	0.9277	41.7946	0.9640	0.9305
11	31.6641	0.6514	0.4830	32.1171	0.9546	0.9132
12	49.1601	0.9662	0.9347	31.6136	0.9740	0.9494
13	70.3672	0.9250	0.8605	33.2454	0.9292	0.8678
14	33.3305	0.9372	0.8818	54.6404	0.9578	0.9190
15	80.2891	0.9719	0.9453	35.6871	0.9733	0.9481
16	30.8211	0.8512	0.7410	30.6975	0.9574	0.9183
17	30.3869	0.8975	0.8140	37.5477	0.9419	0.8901
18	30.6729	0.9387	0.8846	31.1843	0.9407	0.8881
19	32.5207	0.9265	0.8630	30.9910	0.9601	0.9233

20	32.0614	0.8059	0.6749	32.1117	0.8309	0.7107
21	31.5598	0.8908	0.8030	31.5529	0.9427	0.8916
22	31.0172	0.8651	0.7622	31.4436	0.8978	0.8145
23	33.3360	0.9139	0.8414	30.8900	0.9648	0.9320
24	30.9493	0.9704	0.0426	31.5388	0.9756	0.9523
25	32.6568	0.9137	0.8411	31.2372	0.9262	0.8626
26	32.4638	0.7841	0.6448	30.7862	0.8171	0.6908
27	30.7312	0.8476	0.7356	31.0125	0.8374	0.7470
28	30.7196	0.8503	0.7396	31.0420	0.8629	0.7588
29	30.2324	0.9035	0.8242	31.1291	0.9419	0.8375
30	31.0071	0.8046	0.6731	30.4911	0.8163	0.6897
Average	35.3301	0.8497	0.7336	33.1085	0.8821	0.8116

From Table 3 above, by taking the average of the DSC and JSC values for both models in extracting the object's boundaries in all 30 test images, it is observed that the average DSC and JSC values for the proposed model are 0.8821 and 0.8116, respectively, which are 3.81% and 10.63% higher than the average DSC and JSC values recorded in the LSF model. It is also observed that the proposed model is more efficient than the LSF model, as less time was taken to obtain the final segmentation result than the LSF model.

5. CONCLUSION

By integrating the concept of absorbing Markov chain-based saliency image map detection and local image intensities, a new variational global region-based active contour model (AMCSAC) for images with intensity inhomogeneity was introduced in this study. The respective Euler-Lagrange equation was provided to accomplish optimal image segmentation and then solved in MATLAB. Based on segmentation precision and efficiency, the efficacy of the proposed AMCSAC model was compared to other existing models. The average DSC and JSC values were used to evaluate segmentation precision, while processing time was recorded to assess segmentation efficiency. All models could visibly discern the boundaries of the desired objects, but the AMCSAC model had the highest accuracy and efficiency when segmenting images with inhomogeneous intensity. With all these quantitative measures, it has been proven that the saliency image map produced by the AMC method is better than the traditional saliency computation used in [21] and [22]. This is because the saliency maps generated via the AMC method encompass various aspects in any related field to arrive at a more accurate object segmentation. This will benefit several application fields, such as medical imaging, where precise object detection is crucial. Soon, this model will be applied to the formulation of a variational ACM for vector-valued images with intensity heterogeneity and weak boundary problems.

ACKNOWLEDGEMENT

The authors thank GIP Research Grant (Project's code: 600-RMC/GIP 5/3 (078/2022)), Universiti Teknologi MARA, Shah Alam for supporting this research.

CONFLICT OF INTEREST

The authors declare no conflict of interest.

REFERENCES

- [1] S. N. Kumar, A. Lenin Fred, H. Ajay Kumar, and P. Sebastin Varghese, "Performance metric evaluation of segmentation algorithms for gold standard medical images," *Adv. Intell. Syst. and Comput.*, vol. 709, pp. 457–469, 2018.
- [2] N. A. S. M. Ghani, A. K. Jumaat, R. Mahmud, M. A. Maasar, F. A. Zulkifle, and A. M. Jasin, "Breast Abnormality Boundary Extraction in Mammography Image Using Variational Level Set and Self-Organizing Map (SOM)," *Mathematics*, vol. 11, no. 4, pp. 976, Feb. 2023.
- [3] T.C. Saibin and A.K. Jumaat, "Variational selective segmentation model for intensity inhomogeneous image," *Indonesian Journal of Electrical Engineering and Computer Science*, vol. 29, no. 1, pp. 277-285, 2023.
- [4] N. A. S. M. Ghani, A. K. Jumaat, and R. Mahmud, "Boundary Extraction of Abnormality Region in Breast Mammography Image using Active Contours," *ESTEEM Academic Journal*, vol. 18, pp. 115-127, March 2022.
- [5] S. S. Yasiran *et al.*, "Comparison between GVF snake and ED snake in segmenting microcalcifications," *2011 IEEE Conf. Comput. Appl. and Ind. Electron.*, pp. 597–601, Dec. 2011.
- [6] S. S. Yasiran *et al.*, "Microcalcifications segmentation using three edge detection techniques," *Int. Conf. Electron. Devices, Syst., and Appl.*, pp. 207–211, Nov. 2012.
- [7] A. K. Jumaat *et al.*, "Performance comparison of Canny and Sobel edge detectors on Balloon Snake in segmenting masses," *Int. Conf. Comput. and Inf. Sci., ICCOINS 2014 - A Conf. World Eng., Sci. and Technol. Congr., ESTCON 2014 - Proc.*, pp. 1–5, Jun. 2014.
- [8] N. A. K. Zaman, W. E. Z. W. A. Rahman, A. K. Jumaat, and S. S. Yasiran, "Classification of breast abnormalities using artificial neural network," *AIP Conference Proceedings.*, pp. 1–7, 2015.
- [9] M. Kass, A. Witkin, and D. Terzopoulos, "Snakes: Active contour models," *Int. J. comput. vision*, vol. 1, pp. 321–331, 1988.
- [10] S. Osher and J. A. Sethian, "Fronts propagating with curvature-dependent speed: Algorithms based on Hamilton-Jacobi formulations," *J. comput. phys.*, vol. 79, pp. 12–49, 1988.
- [11] H. Ali, L. Rada and N. Badshah, "Image Segmentation for Intensity Inhomogeneity in Presence of High Noise," *IEEE Transactions on Image Processing*, vol. 27, pp. 3729–3738, 2018.
- [12] S. Soomro, A. Munir and K. N. Choi, "Fuzzy c-means clustering based active contour model driven by edge scaled region information," *Expert Syst. with Appl.*, vol. 120, pp. 387–396, 2019.
- [13] A. K. Jumaat and K. Chen, "An Optimization Based Multilevel Algorithm for Variational Image Segmentation Models," *Electron. Trans. Numer. Anal.*, pp. 1–30, 2017.
- [14] A. K. Jumaat and K. Chen, "Three-dimensional convex and selective variational image segmentation model," *Malaysian Journal of Mathematical Sciences.*, vol. 14, no 3, pp. 437–450, 2020.
- [15] D. B. Mumford and J. Shah, "Optimal approximations by piecewise smooth functions and associated variational problems," *Commun. Pure and Appl. Math.*, vol. 42, pp. 577–685, 1989.
- [16] T. F. Chan and L. A. Vese, "Active contours without edges," *IEEE Transactions on Image Processing*, vol. 10, pp. 266–277, 2001.
- [17] C. Li, C. Y. Kao, J. C. Gore and Z. Ding, "Implicit Active Contours Driven by Local Binary Fitting Energy," *Proc. IEEE Conf. Comput. Vision and Pattern Recognit.*, pp. 1–7, 2007.
- [18] K. Zhang, H. Song and L. Zhang, "Active contours driven by local image fitting energy," *Pattern Recognit.*, vol. 43, pp. 1199–1206, 2010.
- [19] H. Wang, and T. Z. Huang, "An adaptive weighting parameter estimation between local and global intensity fitting energy for image segmentation," *Commun in Nonlinear Sci. and Numer. Simul.*, vol. 19, pp. 3098–3105, 2014.
- [20] Y. Yang, W. Jia and B. Wu, "Simultaneous segmentation and correction model for color medical and natural images with intensity inhomogeneity," *The Visual Comput.*, vol. 36, pp. 717–731, 2020.

- [21] E. Iqbal *et. al.*, "Saliency-driven active contour model for image segmentation," *IEEE Access*, vol. 8, pp. 208978–208991, 2020.
- [22] X. H. Zhi and H. B. Shen, "Saliency driven region-edge-based top down level set evolution reveals the asynchronous focus in image segmentation," *Pattern Recognit.*, vol. 80, pp. 241–255, 2018.
- [23] B. Jiang, L. Zhang, H. Lu, C. Yang and M. H. Yang, "Saliency detection via absorbing markov chain." *Proc. IEEE Int. Conf. Comput. Vision*, pp. 1665–1672, 2013.
- [24] N. C. F. Codella *et al.*, "Skin lesion analysis toward melanoma detection: A challenge," *Int. Symposium Biomedical Imaging (ISBI)*, 2018.
- [25] M. Y. Chen *et al.*, "Automatic chinese food identification and quantity estimation," *SIGGRAPH Asia 2012 Technical Briefs*, 2012.